

The Wideband Analysis of the Impact of I/Q Imbalance on THz Communication

Dogus Can Sevdiren¹, Aydin Sezgin¹, and Mohammad Soleymani²

¹ Institute for Digital Communication Systems, Ruhr-Universität Bochum, Germany

² Signal and System Theory Group, Universität Paderborn, Germany

Emails: {dogus.sevdiren, aydin.sezgin}@rub.de, mohammad.soleymani@uni-paderborn.de

Abstract—The terahertz (THz) band is a promising solution to the increasing data traffic demands of future wireless networks. However, developing transceivers for THz communication is a complex and toilsome task due to the difficulty in designing devices that operate at this frequency and the impact of hardware impairments on performance. This paper investigates the impact of radio frequency (RF) impairment, in-phase/quadrature imbalance (IQI). To this end, we express an IQI model for the THz-specific array-of-subarrays (AoSA) architecture considering the unique features of THz communication; vast bandwidth, severe power drawdown, and pencil-like beams. We further model the impact of IQI in the power limited regime in order to investigate the power and ultra-wideband trade-off. To achieve this, we express the spectral efficiency in terms of wideband slope and bit energy to noise ratio which are the two important information theoretic metrics that reveals the performance of the ultra-wideband systems as in THz communication. Our results show that THz systems with IQI have a strict limit in achievable rate although they provide immense spectrum. We also demonstrate with our simulation results that compared to low frequencies, IQI is a more serious concern in THz links.

Index Terms—THz Communication, IQ imbalance, wideband slope

I. INTRODUCTION

The growing reliance on online services has raised expectations for wireless communication systems, driven by a sharp increase in data traffic. Projected wireless network demand is set to exceed one terabit per second, with user-experienced data rates expected to be 10 to 100 times higher. To meet this demand, leveraging the unpolluted terahertz (THz) spectrum is crucial. However, despite significant efforts, developing efficient THz transceivers remains a challenging task.

One significant challenge is the insufficient strength of the signal emitted by antennas operating in the THz band, reported in [1]. Given this power gap, the ultra-wide bandwidth and the decreasing signal strength with distance, the power per unit bandwidth vanishes for THz systems. This case particularly leads THz systems to suffer from lack of power and operate in low signal-to-noise-ratio (SNR) regime. Another important challenge is, obtaining linear hardware response for ultra-wide bandwidth, which in turn introduces severe imperfections in the radio frequency (RF) domain, leads to degradation. One

major impairment reported for the THz transceivers with is the in-phase/quadrature imbalance (IQI) [2]. More precisely, in [3] and [4] attenuation levels around 20 decibel (dB) between in-phase (I) and quadrature (Q) were reported for THz band. For comparison with the conventional frequencies, the Long-Term Evaluation (LTE) standard set forth by 3GPP, stipulated that user equipment must achieve a minimum attenuation of 25 or 28 dB [5].

Some aspects of IQI has been addressed in the state of the art already. For instance, in [6] and in [7] authors discussed IQI for multiple-input-multiple-output (MIMO) systems. In [8], the authors designed improper signals in order to mitigate the impact of IQI. In [2], the THz spatial modulation in the presence of IQI was investigated. In [9], authors proposed a pre-compensation scheme to compensate for nonlinearity and IQI effects. In [10], authors developed a channel estimation and equalization method for THz receivers in the presence of IQI.

This study explores the impact of IQI on a multi-user (MU)-MIMO THz communication system using orthogonal frequency division multiplexing (OFDM) and hybrid beamforming. We employ the wideband slope \mathcal{S}_0 and bit energy-to-noise ratio E_b/N_0 as information-theoretic metrics to assess spectral efficiency (SE) in the low SNR regime, highlighting the challenges posed by the power gap. The paper also compares IQI's effects with inter-user interference (IUI), addressing a gap in existing literature by focusing on ultra-wideband MU-MIMO systems at low power levels for THz communication. This research emphasizes the significant impact of IQI on system performance and the need for further investigation into optimizing power consumption and system efficiency under such conditions.

II. IQI IN MULTICARRIER SYSTEMS

In an OFDM system, the mismatches in the I and Q branches of the local oscillator (LO) signal during up/down conversion can cause interference among subcarriers. For an OFDM signal with $2K$ subcarriers, $k \in \{-K, \dots, -1, 1, \dots, K\}$, where subcarriers are symmetric around the carrier frequency f_c (Fig. 1), IQI results in interference from the symmetric image band during downconversion at the receiver [11] (Fig. 2). Notably, the power of the interfering image band is higher at THz frequencies than at lower

This work was funded by the German Federal Ministry of Education and Research (BMBF) in the course of the 6GEM research hub under grant number 16KISK037.

$$\begin{aligned}
\mathbf{y}[k] = & \mathbf{W}_R[k] (\mathbf{K}_1[k] \mathbf{F}_R^H \mathbf{H}[k] \mathbf{F}_T \mathbf{G}_1[k] + \mathbf{K}_2[k] \mathbf{F}_R^T \mathbf{H}^*[-k] \mathbf{F}_T^* \mathbf{G}_2[k]) \mathbf{W}_T[k] \mathbf{s}[k] \\
& + \mathbf{W}_R[k] (\mathbf{K}_1[k] \mathbf{F}_R^H \mathbf{H}[k] \mathbf{F}_T \mathbf{G}_2^*[k] + \mathbf{K}_2[k] \mathbf{F}_R^T \mathbf{H}^*[-k] \mathbf{F}_T^* \mathbf{G}_1^*[k]) \mathbf{W}_T^*[-k] \mathbf{s}^*[-k] \\
& + \mathbf{W}_R[k] (\mathbf{K}_1[k] \mathbf{z}[k] + \mathbf{K}_2[k] \mathbf{z}^*[-k])
\end{aligned} \tag{3}$$

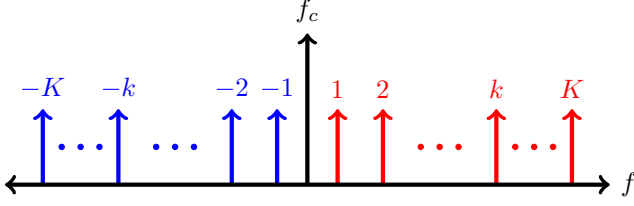


Fig. 1: Subcarrier indexing on passband

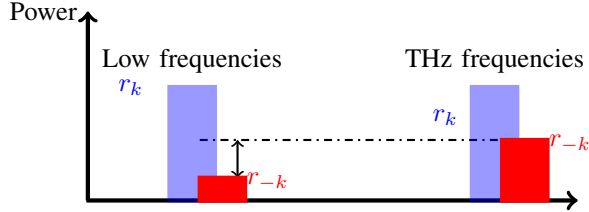


Fig. 2: Comparison of IQI between THz and low frequencies

frequencies, and the same issue occurs during upconversion at the transmitter

III. SYSTEM MODEL

Consider a MU-MIMO OFDM broadcast channel, where transceivers have the structure of array-of-subarrays (AoSA) [12], with a transmitter equipped with N SAs and M single SA users. An SA is composed of Q antenna elements (AE)s where each AE has its own phase shifter and it is linked to a dedicated RF chain. We can express received passband signal $\mathbf{r} \in \mathbb{C}^{MQ \times 1}$ as

$$\mathbf{r}[k] = \mathbf{H}[k] \mathbf{x}[k] + \mathbf{z}[k], \tag{1}$$

where k denotes the subcarrier index out of the $2K$ subcarriers depicted in the Fig. 1. Taking into account the presence of IQI in both the transmitter and receiver, we can represent the transmitted passband signal and the received baseband signal as,

$$\mathbf{x}[k] = \mathbf{F}_T (\mathbf{G}_1[k] \mathbf{W}_T[k] \mathbf{s}[k] + \mathbf{G}_2^*[k] \mathbf{W}_T^*[-k] \mathbf{s}^*[-k]), \tag{2a}$$

$$\mathbf{y}[k] = \mathbf{W}_R[k] (\mathbf{K}_1[k] \mathbf{F}_R^H \mathbf{r}[k] + \mathbf{K}_2[k] \mathbf{F}_R^T \mathbf{r}^*[-k]). \tag{2b}$$

Here, $\mathbf{W}_R \in \mathbb{C}^{M \times M}$ and $\mathbf{F}_R \in \mathbb{C}^{MQ \times M}$, respectively, represent the digital and analog combiners, at the receiver side $\mathbf{W}_T \in \mathbb{C}^{N \times N}$ and $\mathbf{F}_T \in \mathbb{C}^{NQ \times N}$, respectively, indicate the digital and analog beamformers, at the transmitter side. $\mathbf{H} \in \mathbb{C}^{MQ \times NQ}$ is the THz channel matrix, and $\mathbf{z} \in \mathbb{C}^{MQ \times 1}$ is the circularly symmetric complex Gaussian noise vector. Moreover, the transmit symbol vector is denoted by. The overall system model is given in (3) at the top of the page.

The matrices, \mathbf{G}_1 , \mathbf{G}_2 , \mathbf{K}_1 , and \mathbf{K}_2 capture the amplitude and rotational imbalance associated with the transmitter and receiver, respectively, and are given by [11]

$$\mathbf{G}_1 = \frac{1}{2} (\mathbf{I} + \mathbf{G}_T e^{j\Phi_T}), \tag{4a}$$

$$\mathbf{G}_2 = \mathbf{I} - \mathbf{G}_1^*, \tag{4b}$$

$$\mathbf{K}_1 = \frac{1}{2} (\mathbf{I} + \mathbf{G}_R e^{-j\Phi_R}), \tag{4c}$$

$$\mathbf{K}_2 = \mathbf{I} - \mathbf{K}_1^*, \tag{4d}$$

where \mathbf{I} is the identity matrix. The matrices \mathbf{G}_T and \mathbf{G}_R reflect the amplitude errors, Φ_T and Φ_R reflect the phase errors at the transmitter and receiver, respectively. The error matrices are diagonal and given as [6]

$$\mathbf{G}_x = \text{diag}\{g_{x,1}, g_{x,2}, \dots, g_{x,N_x}\}, \tag{5a}$$

$$\Phi_x = \text{diag}\{\Phi_{x,1}, \Phi_{x,2}, \dots, \Phi_{x,N_x}\}, \tag{5b}$$

where x can be T or R , denoting the transmitter and receiver sides, respectively. A system with perfect IQ response is represented by the values $g_{x,i} = 1$ and $\Phi_{x,i} = 0$.

A. Terahertz Channels

THz channels have been widely studied in the literature [13]. Signal propagation in the THz band is mainly dominated by a few reflection paths, with accompanying significant attenuation. As a result, THz channels are primarily influenced and modeled by the line-of-sight (LOS) path, and the channel between the n -th transmit SA and the m -th user can be written as [13]

$$\mathbf{H}_{mn}(f, \Delta) = \alpha_{mn}(f, \Delta) \mathbf{a}_r(\phi_{mn}^a, \theta_{mn}^a) \mathbf{a}_t^H(\phi_{mn}^d, \theta_{mn}^d) \tag{6}$$

where α_{mn} denotes the path loss, \mathbf{a}_r and \mathbf{a}_t represent the receive and transmit antenna steering vectors, respectively. ϕ_a , θ_a and ϕ_d , θ_d denote the angles of arrival (AoA) and the angles of departure (AoD), respectively where ϕ corresponds to azimuth and θ corresponds to elevation. The path loss can be expressed as follows

$$\alpha_{mn} = G_T G_R \frac{c}{4\pi f \Delta} \tag{7}$$

f represents frequency, and Δ denotes the distance between the n -th transmit SA and the m -th user. Sequentially, G_T and G_R indicate the antenna gains of the transmitter and receiver.

Furthermore, we assume that the communication nodes have perfect spatio knowledge. In this case, the optimal analog beamformer between the m -th user and the n -th transmit SA is expressed using the array steering vector of the corresponding SAs

$$\mathbf{f}_r^m = \mathbf{a}_r(\phi_{mn}^a, \theta_{mn}^a), \quad (8a)$$

$$\mathbf{f}_t^n = \mathbf{a}_t^*(\phi_{mn}^d, \theta_{mn}^d), \quad (8b)$$

where \mathbf{f}_r^m is the m -th column of the receive analog combiner \mathbf{F}_R , and \mathbf{f}_t^n is the n -th column of analog beamformer \mathbf{F}_T . The array steering vector of a uniform rectangular planar array (URPA) is [13]

$$\mathbf{a}_0(\phi_0, \theta_0) = \frac{1}{\sqrt{Q}} [e^{jk\Phi_{1,1}}, \dots, e^{jk\Phi_{u,v}}, \dots, e^{jk\Phi_{Q,Q}}], \quad (9)$$

where $\Phi_{u,v}$ is the phase shift of the AE (u, v) and given as

$$\begin{aligned} \Phi_{u,v}(\phi_0, \theta_0) = & s_x^{u,v} \cos \phi_0 \sin \theta_0 \\ & + s_y^{u,v} \cos \phi_0 \sin \theta_0 + s_z^{u,v} \cos \theta_0, \end{aligned} \quad (10)$$

where s_x, s_y, s_z denoting the location of the corresponding AE in the directions x, y and z of the 3D coordinate system, respectively.

The THz channel between the transmit and receive SAs exhibits high correlation due to the dominant line-of-sight (LOS) path and the small size of the antennas, leading to a rank-deficient channel matrix. By exploiting this rank deficiency and utilizing optimal beamforming, the channel dimensions between the transmitter and receiver can be reduced to those of a MIMO channel. This is achieved by concatenating the analog domain components, i.e., the channel and the analog beamformers, as

$$\mathbf{H}_c[k] = \mathbf{F}_R^H \mathbf{H}[k] \mathbf{F}_T, \quad (11)$$

B. Rate Expression with IQI

The signal-to-interference-plus-noise ratio (SINR) serves as the key metric for assessing the performance of a communication system in high SNR regime and IQI introduces additional interference, as shown in Fig. 2. In (3), one can notice that the received signal consists of three components, the signal of the desired sub-carrier $\mathbf{s}[k]$, inter-carrier interference (ICI) $\mathbf{s}[-k]$, and the noise $\mathbf{z}[k]$. Hence, we can split the signal model into two parts, by separating the channel of the desired signal and the channel of the ICI. The channel of the desired sub-carrier signal is

$$\mathbf{H}_d[k] = \mathbf{K}_1 \mathbf{H}_c[k] \mathbf{G}_1 + \mathbf{K}_2 \mathbf{H}_c[-k]^* \mathbf{G}_2, \quad (12)$$

and the channel of the ICI is

$$\mathbf{H}_i[k] = \mathbf{K}_1 \mathbf{H}_c[k] \mathbf{G}_2^* + \mathbf{K}_2 \mathbf{H}_c[-k]^* \mathbf{G}_1^*. \quad (13)$$

Finally, we can define the rate of the k -th subcarrier by

$$R[k] = \log_2 |\mathbf{I} + \mathbf{C}^{-1} \mathbf{W}_R^H \mathbf{H}_d \mathbf{W}_T[k] \mathbf{W}_T^H[k] \mathbf{H}_d^H \mathbf{W}_R|, \quad (14)$$

where $s[k]$ is circularly symmetric complex gaussian with $s[k] \sim \mathcal{N}(0, \mathbf{I})$. Here we treat interference as noise and the corresponding interference plus noise covariance matrix \mathbf{C} is defined as

$$\mathbf{C} = \mathbf{W}_R \mathbf{H}_i \mathbf{W}_T[-k]^* \mathbf{W}_T[-k]^T \mathbf{H}_i^H \mathbf{W}_R + \bar{\mathbf{Z}}, \quad (15)$$

where $\bar{\mathbf{Z}}$ denotes the noise covariance matrix with IQI, and written as

$$\bar{\mathbf{Z}} = \frac{\sigma^2}{2} (\mathbf{I} + \mathbf{G}_T \mathbf{G}_T^H) \quad (16)$$

with

$$E\{\mathbf{z}^H[k] \mathbf{z}[k]\} = \sigma^2 \mathbf{I}, \quad (17)$$

where \mathbf{I} to be equal to identity matrix and G_x is drawn from amplitude error matrix of (5) for the receiver. We can observe from the covariance matrix of interference give in (15) that, the source of the interference is the signal located at the image frequency. In order to mitigate the interference due to IQI, the subcarrier associated with the image frequency can be nulled which implies that no signal is being transmitted on this specific subcarrier.

IV. WIDEBAND ANALYSIS

In ultra-wideband systems in the power limited regime, the power per unit bandwidth diminishes around zero and system operates in low SNR regime. In this regime, the key measure for the system performance is the energy-per-information bit developed by Verdú in [14], where SE is formulated in terms of energy per bit normalized to background noise spectral level E_b/N_0 as

$$\text{SE} \left(\frac{E_b}{N_0} \right) \approx S_0 \frac{\frac{E_b}{N_0} (\text{dB}) - \frac{E_b}{N_{0,\min}} (\text{dB})}{3\text{dB}}. \quad (18)$$

Here, $E_b/N_{0,\min}$ is the minimum achievable energy per bit, and S_0 is the wideband slope.

A. Wideband Slope in the Absence of IQI

We first derive the wideband slope and minimum achievable energy per bit of THz communication link in the absence of IQI. In [15], the authors presented a model for interference channels in low-SNR regime. By exploiting this model, we can express the minimum achievable energy per bit for the system without IQI. We can write the system without IQI as

$$\mathbf{y}[k] = \mathbf{W}_R[k] \mathbf{H}_c[k] \mathbf{W}_T[k] \mathbf{s}[k] + \mathbf{W}_R[k] \mathbf{z}[k], \quad (19)$$

where \mathbf{H}_c is the concatenated channel given in (11). For this system we can express the SINR of the k -th subcarrier for m -th user by treating interference as noise and under the equal power constraint as

$$\gamma_m[k] = \frac{|h_{c,mm}[k]|^2 P}{P \sum_{n \neq m} |h_{c,mn}[k]|^2 + \sigma^2}, \quad (20)$$

where P is the power, $h_{c,mm}$ is the element in the m -th row and n -th column of \mathbf{H}_c . Under the unitary noise power assumption, see [15], we can express the minimum achievable energy per bit as

$$\frac{E_b}{N_{0,\min}} = \frac{N2K \log_e 2}{\sum_{k \neq 0}^K \sum_{m=1}^M |h_{c,mm}[k]|^2}, \quad (21)$$

and the wideband slope as

$$S_0 = \frac{2 \left(\sum_{\substack{k=-K \\ k \neq 0}}^K \sum_{m=1}^M |h_{c,mm}[k]|^2 \right)^2}{\sum_{\substack{k=-K \\ k \neq 0}}^K \sum_{m=1}^M \left(|h_{c,mm}[k]|^4 + \sum_{\substack{n=1 \\ i \neq m}}^N |h_{c,mm}[k]|^2 |h_{c,mn}[k]|^2 \right)}. \quad (22)$$

B. Wideband Slope in the Presence of IQI

We now extend this model to account for the presence of IQI and resulting interference. The minimum achievable energy per bit is affected by the presence of IQI. We can express the SINR of the k -th subcarrier for m -th user by treating interference as noise and under the equal power constraint as

$$\gamma_m[k] = \frac{|h_{d,mm}[k]|^2 P}{P \left(\sum_{n \neq m} |h_{d,mn}[k]|^2 + \sum_{n=1}^{n=N} |h_{i,mn}[k]|^2 \right) + \sigma^2}, \quad (23)$$

Here subscript d denotes the entries of the desired signal channel matrix \mathbf{H}_d given in (12), and subscript i denotes the entries of the interference signal channel matrix \mathbf{H}_i given in (13). Similarly, m denotes the row, and n denotes the column corresponding to the user and transmit SAs, respectively. By comparing (23) with (20), we can observe that IQI superpose an additional interference and modifies the end-to-end analog properties of the system, hence the channel. Under the same assumptions, we can express the minimum achievable energy per bit as

$$\frac{E_b}{N_{0,\min}} \Big|_{IQI} = \frac{N^2 K \log_e 2}{\sum_{\substack{k=-K \\ k \neq 0}}^K \sum_{m=1}^M |h_{d,mm}[k]|^2}, \quad (24)$$

and the wideband slope as

$$S_0 \Big|_{IQI} = 2 \frac{\left(\sum_{\substack{k=-K \\ k \neq 0}}^K \sum_{m=1}^M |h_{d,mm}[k]|^2 \right)^2}{\sum_{\substack{k=-K \\ k \neq 0}}^K \sum_{m=1}^M \left(|h_{d,mm}[k]|^4 + \zeta_m \right)}, \quad (25)$$

with

$$\zeta_m = \sum_{\substack{n=1 \\ n \neq m}}^N |h_{d,mm}[k]|^2 |h_{d,mn}[k]|^2 + \sum_{n=1}^N |h_{d,mm}[k]|^2 |h_{i,mn}[k]|^2, \quad (26)$$

where ζ_m represents the additional interference terms due to IQI.

V. NUMERICAL SIMULATION

In the simulations, we consider a system communicating at 300 GHz. We employ a transmitter with three SAs; and three single SA users. The results can be extended to multi-SA user cases without loss of generality. The number of antenna elements on a single SA is 256, i.e., $Q = 16$, $N = 3$, and $M = 3$. We use a bandwidth of 10 GHz. In each simulation, users are located at arbitrary locations at a certain distance.

A. Result of Impact of IQI on Wideband Slope

This subsection presents simulation results demonstrating the impact of IQI on a wideband, power-limited system. Specifically, Fig. 3 shows the achievable wideband slope with respect to IQI, measured in terms of amplitude imbalance. This can be interpreted as the system's benefit per unit of resource (e.g., power or bandwidth) in the presence of IQI. Lower values of g indicate higher levels of IQI. The slope curve reveals that as IQI becomes more severe, the benefit the system get from increasing resources significantly diminishes.

Similarly, Fig. 4 illustrates the impact of the IQI on SE. In this figure, each curve corresponds to a different amplitude imbalance, i.e. solid black line shows $g = 0.9$, the blue dashed line shows $g = 0.8$, and the red dotted line shows $g = 0.7$. As it can be observed, as the IQI becomes more severe, the bit energy required for the same performance is significantly increased.

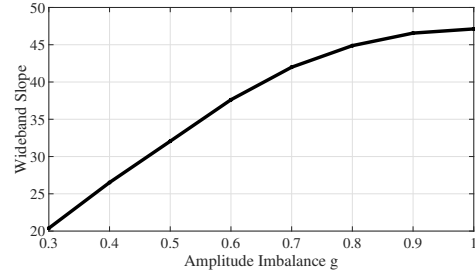


Fig. 3: Wideband Slope vs. Amplitude Impairment

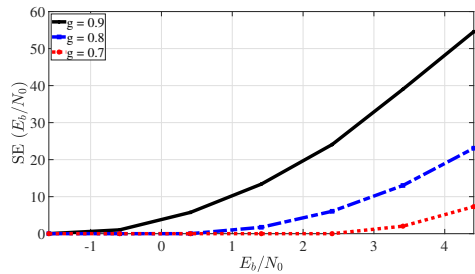


Fig. 4: Spectral Efficiency vs. E_b/N_0

B. Analysis of IQI and Subcarrier Nulling

This subsection examines the impact of IQI and subcarrier nulling on data rates in THz systems, using a phase imbalance of 5° and an image rejection ratio of 30 dB, as specified in [3]. We analyze systems with and without IUI, using Rayleigh fading for conventional frequencies.

Fig. 5 shows the relationship between achievable data rates and power, given in SNR, in the presence of ICI from IQI

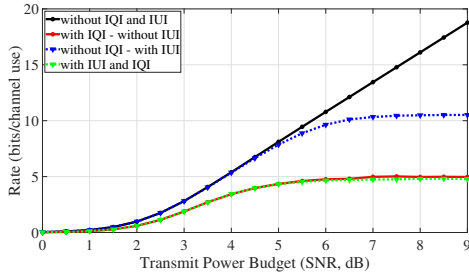


Fig. 5: Impact of IQI on rate in THz band

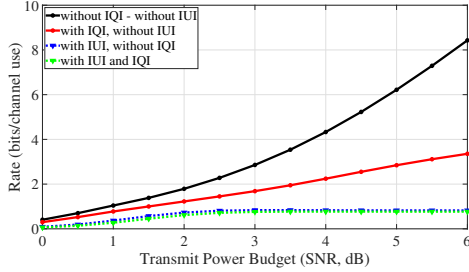


Fig. 6: Impact of IQI on rate in Low Frequencies

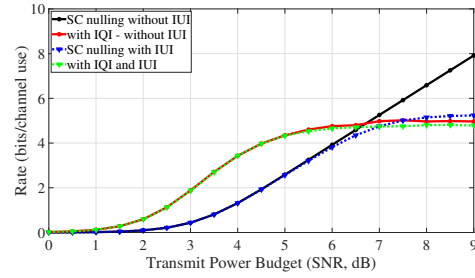


Fig. 7: Subcarrier nulling THz band

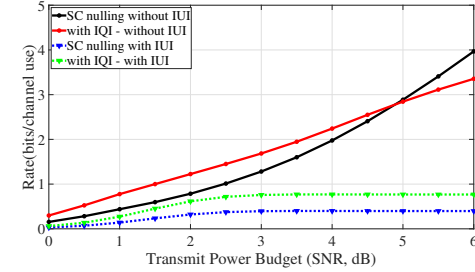


Fig. 8: Subcarrier nulling in Low Frequencies

and IUI. The solid black line indicates the rate without interference, showing a steady increase with power. The red line, with IQI, saturates as power increases due to growing IQI interference. The blue dashed line with IUI limits the achievable rate, while the red and green dashed lines (IQI only and joint IQI/IUI) overlap, suggesting IQI is more severe than IUI in THz systems. In contrast, Fig. 6 shows that IUI is more problematic at lower frequencies, where systems can achieve higher rates despite IQI.

To mitigate IQI, we propose subcarrier nulling, where power is allocated to the subcarrier k but not to the $-k$ -th subcarrier, effectively halving the bandwidth to avoid intercarrier interference. Figs. 7 and 8 show that subcarrier nulling consistently outperforms using the full bandwidth, particularly in THz systems where IUI is negligible.

An important finding is that, despite the abundant THz spectrum, data rates do not consistently increase with bandwidth when IQI is present. Using half the bandwidth can be more effective, highlighting IQI as a key obstacle to achieving THz communication's potential.

VI. CONCLUSION

This research examines IQI in THz communication systems, highlighting its significant challenge and the need for effective mitigation strategies. Our analysis of power-limited wideband systems reveals the negative impact of IQI on spectral efficiency, emphasizing the need for further research to develop mitigation techniques and fully unlock the potential of THz networks for ultra-high data rates.

REFERENCES

[1] J. Blackledge, A. Boretti, L. Rosa, and S. Castelletto, "Fractal graphene patch antennas and the thz communications revolution," in *IOP Conf. Ser.: Mat. Sci. and Eng.*, vol. 1060, no. 1, 2021, p. 012001.

[2] T. Mao, Q. Wang, and Z. Wang, "Spatial modulation for terahertz communication systems with hardware impairments," *IEEE Trans. Veh. Technol.*, vol. 69, no. 4, pp. 4553–4557, 2020.

[3] H.-J. Song, J.-Y. Kim, K. Ajito, N. Kukutsu, and M. Yaita, "50-gb/s direct conversion QPSK modulator and demodulator MMICs for terahertz communications at 300 GHz," *IEEE Trans. Microw. Theory Tech.*, vol. 62, no. 3, pp. 600–609, 2014.

[4] P. R. Vazquez, J. Grzyb, N. Sarmah, B. Heinemann, and U. R. Pfeiffer, "A 219–266 GHz fully-integrated direct-conversion IQ receiver module in a SiGe HBT technology," in *EuMIC*, 2017, pp. 261–264.

[5] D. Korpi, L. Anttila, V. Syrjälä, and M. Valkama, "Widely linear digital self-interference cancellation in direct-conversion full-duplex transceiver," *IEEE Journ. on Sel. Areas in Commun.*, vol. 32, no. 9, pp. 1674–1687, 2014.

[6] S. Javed, O. Amin, S. S. Ikki, and M.-S. Alouini, "Multiple antenna systems with hardware impairments: New performance limits," *IEEE Trans. Veh. Technol.*, vol. 68, no. 2, pp. 1593–1606, 2019.

[7] M. Soleymani, I. Santamaria, B. Maham, and P. J. Schreier, "Rate region of the k-user mimo interference channel with imperfect transmitters," in *EUSIPCO*, 2021, pp. 1638–1642.

[8] M. Soleymani, I. Santamaria, A. Sezgin, and E. Jorswieck, "Maximizing spectral and energy efficiency in multi-user mimo ofdm systems with ris and hardware impairment," *arXiv preprint arXiv:2401.11921*, 2024.

[9] Y. R. Ramadan, H. Minn, and M. E. Abdelgelil, "Precompensation and system parameters estimation for low-cost nonlinear terahertz transmitters in the presence of I/Q imbalance," *IEEE Access*, vol. 6, pp. 51 814–51 833, 2018.

[10] Z. Sha and Z. Wang, "Channel estimation and equalization for terahertz receiver with RF impairments," *IEEE Journ. on Sel. Areas in Commun.*, vol. 39, no. 6, pp. 1621–1635, 2021.

[11] T. C. Schenk, P. F. Smulders, and E. R. Fledderus, "Estimation and compensation of TX and RX IQ imbalance in OFDM-based MIMO systems," in *IEEE Radio and Wireless Sym.*, 2006, pp. 215–218.

[12] C. Lin and G. Y. L. Li, "Terahertz communications: An array-of-subarrays solution," *IEEE Commun. Mag.*, vol. 54, no. 12, pp. 124–131, 2016.

[13] H. Sarrideen, M.-S. Alouini, and T. Y. Al-Naffouri, "An overview of signal processing techniques for terahertz communications," *Proceedings of the IEEE*, vol. 109, no. 10, pp. 1628–1665, 2021.

[14] S. Verdú, "Spectral efficiency in the wideband regime," *IEEE Trans. on Inf. Theory*, vol. 48, no. 6, pp. 1319–1343, 2002.

[15] M. Shen and A. Høst-Madsen, "The wideband slope of interference channels: The small bandwidth case," *IEEE Trans. on Inf. Theory*, vol. 65, no. 11, pp. 7287–7303, 2019.